R E M A R K S

Reconsideration of this application, as amended, is respectfully requested.

ALLOWABLE SUBJECT MATTER

The Examiner's indication of the allowability of the subject matter of claims 9, 18, 27 and 36 is again respectfully acknowledged.

These claims, however, have again not been rewritten in independent form at this time since, as set forth in detail hereinbelow, it is respectfully submitted that their respective parent claims, as amended, also recite allowable subject matter.

THE CLAIMS

Independent claims 1, 10, 19 and 28 have been amended to clarify the definition of the Dyadic Wavelet transform recited therein, as well as to clarify the difference between the multi-resolution conversion processing (including the Discrete Wavelet transform, such as the bi-orthogonal Wavelet transform, etc.) and the Dyadic Wavelet transform. See the disclosure in the specification at pages 26-42.

No new matter has been added, and it is respectfully requested that the amendments to the claims be approved and entered.

THE PRIOR ART REJECTION

Claims 1-7, 10-16, 19-25 and 28-34 were again rejected under 35 USC 102 as being anticipated by USP 6,823,090 ("Matsuura"); and claims 8, 17, 26 and 35 were again rejected under 35 USC 103 as being obvious over Matsuura in view of USP 6,741,739 ("Vincent"). These rejections, however, are respectfully traversed with respect to the claims as amended hereinabove.

As pointed out hereinabove, independent claims 1, 10, 19 and 28 have been amended to clarify the definition of the Dyadic Wavelet transform recited therein, as well as to clarify the difference between the multi-resolution conversion processing (including the Discrete Wavelet transform, such as the bi-orthogonal Wavelet transform, etc.) and the Dyadic Wavelet transform. In addition, for the Examiner's reference, submitted herewith is a technical document entitled "A WAVELET TOUR OF SIGNAL PROCESSING" which provides background information on the difference between the Discrete Wavelet transform, such as the bi-orthogonal Wavelet transform, etc., and the Dyadic Wavelet transform.

According to the present invention as recited in amended independent claim 1, for example, a method for processing image signals is provided which comprises:

reading an image recorded on a recording medium so as to generate image signals representing the image;

applying, to the image signals, a multi-resolution conversion processing of at least level 1, which is capable of reducing an image size of the image signals, so as to generate first-converted image signals from the image signals; and

applying a Dyadic Wavelet transform of at least level 1 to lowest frequency band component signals included in the first-converted image signals, so as to generate second-converted image signals from the first-converted image signals;

wherein no down-sampling is performed in the Dyadic Wavelet transform, and wavelet function $\Psi_{i,j}(x)$ to be employed in the Dyadic Wavelet transform is defined by an equation shown below:

$$\psi_{i,j}(x) = 2^{-i}\,\psi\left(\frac{x-j}{2^{i}}\right)$$

where "i" denotes a natural number; and

wherein an image size of said first-converted image signals is smaller than the image size of said image signals, while an image size of said second-converted image signals is identical to the image size of said first-converted image signals.

Amended independent claims 10, 19, and 28, moreover, recite corresponding apparatuses and a computer program having essentially the same claimed features as above described amended independent claim 1.

With the structure of the claimed present invention as recited in the amended independent claims, the multi-resolution conversion processing of at least level 1 (for instance, the bi-orthogonal wavelet transform) is applied to the image signals read from the original image, so as to generate the first-converted image signals from the image signals. Successively, the Dyadic Wavelet transform (instead of the Discrete Wavelet transform, such as the bi-orthogonal wavelet transform) of at least level 1 is applied to the lowest frequency band component signals extracted from the first-converted image signals.

It is noted "multi-resolution conversion processing" is described in the specification of the present application from page 26, line 16 to page 34, line 18, and that the "Dyadic Wavelet transform" is described in the specification from page 34, line 19 to page 42, line 23. As is apparent from a comparison between the definitions of the multi-resolution conversion processing and the Dyadic Wavelet transform as described in the specification of the present application, the down-sampling (equivalent to a sub-sampling operation defined in the technical document entitled "A WAVELET TOUR OF SIGNAL PROCESSING") is performed in the bi-orthogonal wavelet transform as shown in Fig. 2 and Fig. 3, and accordingly, the image size is reduced after applying the bi-orthogonal wavelet transform. On the other hand, no down-sampling is performed in the Dyadic

Wavelet transform as shown in Fig. 7 and Fig. 8, and accordingly, the image size is maintained as the same between before and after applying the Dyadic Wavelet transform. Still further, the wavelet function $g_{i,3}(x)$ to be employed in the bi-orthogonal wavelet transform, defined by Equation 4 shown on page 29, line 1 of the specification of the present application, is completely different for that to be employed in the Dyadic Wavelet transform, defined by Equation 8 on page 35, line 6 of the specification of the present application. Therefore, according to the claimed present invention, two completely different processings, namely, the multi-resolution conversion processing and the Dyadic Wavelet transform, are successively applied to the image signals, so as to generate second-converted image signals.

In addition, it is noted that image processing is applied only to the high frequency band component signals acquired by applying the multi-resolution conversion processing and the Dyadic Wavelet transform. Thus, according to the claimed present invention, it becomes possible to reduce the processing load without causing a deterioration of the image quality. And as a result, the advantageous effects described in the specification from page 74, line 20 to page 75, line 15 can be achieved.

It is respectfully submitted that the structural features and advantageous effects of the claimed present invention are

simply not at all disclosed, taught, or suggested by any of the cited prior art references or any combination thereof.

In particular, it is respectfully noted that Matsuura discloses an IMAGE PROCESSING APPARATUS AND METHOD in which a discrete wavelet transform is applied to original X-ray image signals, so as to reduce the noise components included in the original X-ray image signals. On page 2 of the Final Office Action, the Examiner strongly asserts that the discrete wavelet transform used by Matsuura is a dyadic wavelet transform, and further, points out again that the discrete wavelet transform disclosed by Matsuura is Dyadic, by using bold letters.

However, judging from the disclosure at column 5, line 53 to column 6, line 16 of Matsuura, it is apparent that the discrete wavelet transform disclosed by Matsuura is not a Dyadic wavelet transform, but rather is a bi-orthogonal wavelet transform (which is equivalent to that defined by the present specification from page 26, line 16 to page 34, line 18, or the transform described at pages 255-269 of the technical document entitled "A WAVELET TOUR OF SIGNAL PROCESSING" submitted herewith). This is because in the discrete wavelet transformation circuit 116 of Matsuura, a subsampling, such as a down-sampling and an up-sampling, is implemented to achieve the bi-orthogonal wavelet transform or the inverse bi-orthogonal wavelet transform. If the discrete wavelet transform disclosed by Matsuura were a Dyadic wavelet transform,

such subsampling would not be implemented, as is apparent from the definitions described in the specification of the present application from page 34, line 19 to page 42, line 23, or the definitions described at pages 148-157 of the technical document entitled "A WAVELET TOUR OF SIGNAL PROCESSING" submitted herewith. Indeed, it is respectfully submitted that Matsuura does not use the term of "Dyadic Wavelet transform" and does not at all describe a Dyadic Wavelet transform.

Still further, it is respectfully submtited that Matsuura completely fails to disclose a process for "applying a Dyadic Wavelet transform of at least level 1 to lowest frequency band component signals included in the first-converted image signals, so as to generate second-converted image signals from the first-converted image signals," as according to the claimed present invention. Instead, Matsuura merely discloses the conventional method for applying the bi-orthogonal wavelet transform, being a kind of Discrete Wavelet transform, to the original X-ray image signals according to the conventionally well known process, so as to reduce the noise components included in the original X-ray image signals.

Accordingly, it is respectfully submitted that the method and apparatus of Matsuura cannot attain the advantageous effects achieved by the claimed present invention described in the

specification of the present application from page 74, line 14 to page 75, line 15.

It is respectfully submitted, moreover, that Vincent also fails to disclose, teach or suggest the above described structural features and advantageous effects of the claimed present invention.

Accordingly, it is respectfully submitted that amended independent claims 1, 10, 19 and 28, and claims 2-9, 11-18, 20-27 and 29-36 respectively depending therefrom, all clearly patentably distinguish over Matsuura and Vincent, taken singly or in combination, under 35 USC 102 as well as under 35 USC 103.

* *

Entry of this Amendment, allowance of the claims and the passing of this application to issue are respectfully solicited.

If the Examiner has any comments, questions, objections or recommendations, the Examiner is invited to telephone the undersigned for prompt action.

Respectfully submitted,

/Douglas Holtz/

Douglas Holtz
Reg. No. 33,902

Frishauf, Holtz, Goodman & Chick, P.C.
220 Fifth Avenue - 16th Floor
New York, New York 10001-7708
Tel. No. (212) 319-4900
DH:
encs.

A WAVELET TOUR OF SIGNAL PROCESSING

Second Edition

Stéphane Mallat

École Polytechnique, Paris

Courant Institute, New York University

ACADEMIC PRESS

This book is printed on acid-free paper. ♾

ACADEMIC PRESS
A Harcourt Science and Technology Company
525 B Street, Suite 1900, San Diego, CA 92101-4495, USA
1300 Boylston Street, Chestnut Hill, MA 02167, USA
http://www.academicpress.com

Academic Press
A Harcourt Science and Technology Company
Harcourt Place, 32 Jamestown Road, London NW1 7BY, UK
http://www.academicpress.com

ISBN 0-12-466606-X

A catalogue record for this book is available from the British Library

Library of Congress Catalog Card Number: 99-65087

A mes parents,
Alexandre et Francine

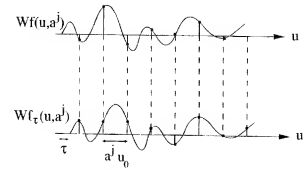

FIGURE 5.3 If $f_\tau(t) = f(t-\tau)$ then $Wf_\tau(u,a^j) = Wf(u-\tau,a^j)$. Uniformly sampling $Wf_\tau(u,a^j)$ and $Wf(u,a^j)$ at $u = na^j u_0$ may yield very different values if $\tau \neq ku_0a^j$.

Translation-Invariant Representations There are several strategies for maintaining the translation invariance of a wavelet transform. If the sampling interval $a^j u_0$ is small enough then the samples of $f \star \psi_{a^j}(t)$ are approximately translated when f is shifted. The dyadic wavelet transform presented in Section 5.5 is a translation-invariant representation that does not sample the translation factor u. This creates a highly redundant signal representation.

To reduce the representation size while maintaining translation invariance, one can use an adaptive sampling scheme, where the sampling grid is automatically translated when the signal is translated. For each scale a^j, $Wf(u,a^j) = f \star \bar{\psi}_{a^j}(u)$ can be sampled at locations u where $|Wf(a^j,u)|$ is locally maximum. The resulting representation is translation invariant since the local maxima positions are translated when f and hence $f \star \bar{\psi}_{a^j}$ are translated. This adaptive sampling is studied in Section 6.2.2.

5.5 DYADIC WAVELET TRANSFORM [2]

To construct a translation-invariant wavelet representation, the scale s is discretized but not the translation parameter u. The scale is sampled along a dyadic sequence $\{2^j\}_{j\in\mathbb{Z}}$, to simplify the numerical calculations. Fast computations with filter banks are presented in the next two sections. An application to computer vision and texture discrimination is described in Section 5.5.3.

The dyadic wavelet transform of $f \in \mathbf{L}^2(\mathbb{R})$ is defined by

$$Wf(u,2^j) = \int_{-\infty}^{+\infty} f(t)\,\frac{1}{\sqrt{2^j}}\,\psi\left(\frac{t-u}{2^j}\right)dt = f \star \bar{\psi}_{2^j}(u), \tag{5.67}$$

with

$$\bar{\psi}_{2^j}(t) = \psi_{2^j}(-t) = \frac{1}{\sqrt{2^j}}\,\psi\left(\frac{-t}{2^j}\right).$$

The following proposition proves that if the frequency axis is completely covered by dilated dyadic wavelets, as illustrated by Figure 5.4, then it defines a complete and stable representation.

Theorem 5.11 *If there exist two constants $A > 0$ and $B > 0$ such that*

$$\forall \omega \in \mathbb{R} - \{0\}\ ,\ A \leq \sum_{j=-\infty}^{+\infty} |\hat{\psi}(2^j\omega)|^2 \leq B, \tag{5.68}$$

then

$$A\|f\|^2 \leq \sum_{j=-\infty}^{+\infty} \frac{1}{2^j}\,\|Wf(u,2^j)\|^2 \leq B\|f\|^2. \tag{5.69}$$

If $\tilde{\psi}$ satisfies

$$\forall \omega \in \mathbb{R} - \{0\}\ ,\ \sum_{j=-\infty}^{+\infty} \hat{\psi}^*(2^j\omega)\,\hat{\tilde{\psi}}(2^j\omega) = 1, \tag{5.70}$$

then

$$f(t) = \sum_{j=-\infty}^{+\infty} \frac{1}{2^j}\,Wf(.,2^j) \star \tilde{\psi}_{2^j}(t). \tag{5.71}$$

Proof [2]. The Fourier transform of $f_j(u) = Wf(u,2^j)$ with respect to u is derived from the convolution formula (5.67):

$$\hat{f}_j(\omega) = \sqrt{2^j}\,\hat{\psi}^*(2^j\omega)\,\hat{f}(\omega). \tag{5.72}$$

The condition (5.68) implies that

$$A|\hat{f}(\omega)|^2 \leq \sum_{j=-\infty}^{+\infty} \frac{1}{2^j}\,|\hat{f}_j(\omega)|^2 \leq B\,|\hat{f}(\omega)|^2.$$

Integrating each side of this inequality with respect to ω and applying the Parseval equality (2.25) yields (5.69).

Equation (5.71) is proved by taking the Fourier transform on both sides and inserting (5.70) and (5.72). ■

The energy equivalence (5.69) proves that the normalized dyadic wavelet transform operator

$$Uf[j,u] = \frac{1}{\sqrt{2^j}}\,Wf(u,2^j) = \left\langle f, \frac{1}{\sqrt{2^j}}\,\psi_{2^j}(t-u)\right\rangle$$

satisfies frame inequalities. There exist an infinite number of reconstructing wavelets $\tilde{\psi}$ that verify (5.70). They correspond to different left inverses of U, calculated with (5.71). If we choose

$$\hat{\tilde{\psi}}(\omega) = \frac{\hat{\psi}(\omega)}{\sum_{j=-\infty}^{+\infty} |\hat{\psi}(2^j\omega)|^2}, \tag{5.73}$$

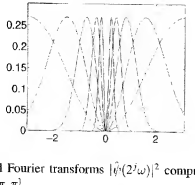

FIGURE 5.4 Scaled Fourier transforms $|\hat{\psi}(2^j\omega)|^2$ computed with (5.84), for $1 \leq j \leq 5$ and $\omega \in [-\pi, \pi]$.

then one can verify that the left inverse is the pseudo inverse $\tilde{U}^{-1}$. Figure 5.5 gives a dyadic wavelet transform computed over 5 scales with the quadratic spline wavelet shown in Figure 5.6.

5.5.1 Wavelet Design

A discrete dyadic wavelet transform can be computed with a fast filter bank algorithm if the wavelet is appropriately designed. The synthesis of these dyadic wavelets is similar to the construction of biorthogonal wavelet bases, explained in Section 7.4. All technical issues related to the convergence of infinite cascades of filters are avoided in this section. Reading Chapter 7 first is necessary for understanding the main results.

Let h and g be a pair of finite impulse response filters. Suppose that h is a low-pass filter whose transfer function satisfies $\hat{h}(0) = \sqrt{2}$. As in the case of orthogonal and biorthogonal wavelet bases, we construct a scaling function whose Fourier transform is

$$\hat{\phi}(\omega) = \prod_{p=1}^{+\infty} \frac{\hat{h}(2^{-p}\omega)}{\sqrt{2}} = \frac{1}{\sqrt{2}}\, \hat{h}\left(\frac{\omega}{2}\right) \hat{\phi}\left(\frac{\omega}{2}\right). \tag{5.74}$$

We suppose here that this Fourier transform is a finite energy function so that $\phi \in \mathbf{L}^2(\mathbb{R})$. The corresponding wavelet ψ has a Fourier transform defined by

$$\hat{\psi}(\omega) = \frac{1}{\sqrt{2}}\, \hat{g}\left(\frac{\omega}{2}\right) \hat{\phi}\left(\frac{\omega}{2}\right). \tag{5.75}$$

Proposition 7.2 proves that both ϕ and ψ have a compact support because h and g have a finite number of non-zero coefficients. The number of vanishing moments of ψ is equal to the number of zeroes of $\hat{\psi}(\omega)$ at $\omega = 0$. Since $\hat{\phi}(0) = 1$, (5.75) implies that it is also equal to the number of zeros of $\hat{g}(\omega)$ at $\omega = 0$.

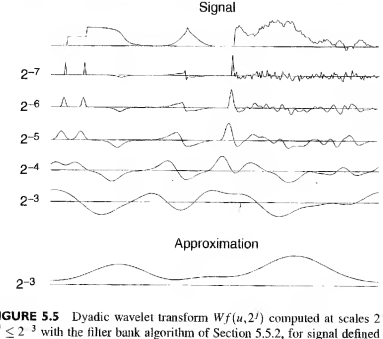

FIGURE 5.5 Dyadic wavelet transform $Wf(u, 2^j)$ computed at scales $2^{-7} \leq 2^j \leq 2^{-3}$ with the filter bank algorithm of Section 5.5.2, for signal defined over $[0, 1]$. The bottom curve carries the lower frequencies corresponding to scales larger than 2^{-3}.

Reconstructing Wavelets Reconstructing wavelets that satisfy (5.70) are calculated with a pair of finite impulse response dual filters $\tilde{h}$ and $\tilde{g}$. We suppose that the following Fourier transform has a finite energy:

$$\hat{\tilde{\phi}}(\omega) = \prod_{p=1}^{+\infty} \frac{\hat{\tilde{h}}(2^{-p}\omega)}{\sqrt{2}} = \frac{1}{\sqrt{2}}\, \hat{\tilde{h}}\left(\frac{\omega}{2}\right) \hat{\tilde{\phi}}\left(\frac{\omega}{2}\right). \tag{5.76}$$

Let us define

$$\hat{\tilde{\psi}}(\omega) = \frac{1}{\sqrt{2}}\, \hat{\tilde{g}}\left(\frac{\omega}{2}\right) \hat{\tilde{\phi}}\left(\frac{\omega}{2}\right). \tag{5.77}$$

The following proposition gives a sufficient condition to guarantee that $\hat{\tilde{\psi}}$ is the Fourier transform of a reconstruction wavelet.

Proposition 5.5 *If the filters satisfy*

$$\forall \omega \in [-\pi, \pi] \ , \ \hat{\tilde{h}}(\omega)\, \hat{h}^*(\omega) + \hat{\tilde{g}}(\omega)\, \hat{g}^*(\omega) = 2 \tag{5.78}$$

then

$$\forall \omega \in \mathbb{R} - \{0\} \ , \ \sum_{j=-\infty}^{+\infty} \hat{\psi}^*(2^j\omega)\, \hat{\tilde{\psi}}(2^j\omega) = 1. \tag{5.79}$$

Proof [2]. The Fourier transform expressions (5.75) and (5.77) prove that

$$\widehat{\psi}(\omega)\hat{\psi}^*(\omega) = \frac{1}{2}\widehat{\bar{g}}\left(\frac{\omega}{2}\right)\hat{g}^*\left(\frac{\omega}{2}\right)\widehat{\phi}\left(\frac{\omega}{2}\right)\hat{\phi}^*\left(\frac{\omega}{2}\right).$$

Equation (5.78) implies

$$\begin{aligned}\widehat{\phi}(\omega)\hat{\psi}^*(\omega) &= \frac{1}{2}\left[2-\widehat{h}\left(\frac{\omega}{2}\right)\hat{h}^*\left(\frac{\omega}{2}\right)\right]\widehat{\phi}\left(\frac{\omega}{2}\right)\hat{\phi}^*\left(\frac{\omega}{2}\right)\\ &= \widehat{\phi}\left(\frac{\omega}{2}\right)\hat{\phi}^*\left(\frac{\omega}{2}\right) - \widehat{\phi}(\omega)\hat{\phi}^*(\omega).\end{aligned}$$

Hence

$$\sum_{l=-k}^{k}\widehat{\psi}(2^l\omega)\hat{\psi}^*(2^l\omega) = \hat{\phi}^*(2^{-l}\omega)\widehat{\phi}(2^{-l}\omega) - \hat{\phi}^*(2^k\omega)\widehat{\phi}(2^k\omega).$$

Since $\hat{g}(0)=0$, (5.78) implies $\widehat{h}(0)\hat{h}^*(0)=2$. We also impose that $\widehat{h}(0)=\sqrt{2}$ so one can derive from (5.74,5.76) that $\widehat{\phi}(0)=\hat{\phi}^*(0)=1$. Since ϕ and $\tilde{\phi}$ belong to $\mathbf{L}^1(\mathbb{R})$, $\hat{\phi}$ and $\widehat{\phi}$ are continuous, and the Riemann-Lebesgue lemma (Problem 2.6) proves that $|\hat{\phi}(\omega)|$ and $|\widehat{\phi}(\omega)|$ decrease to zero when ω goes to ∞. For $\omega\neq 0$, letting k and l go to $+\infty$ yields (5.79). ■

Observe that (5.78) is the same as the unit gain condition (7.122) for biorthogonal wavelets. The aliasing cancellation condition (7.121) of biorthogonal wavelets is not required because the wavelet transform is not sampled in time.

Finite Impulse Response Solution Let us shift h and g to obtain causal filters. The resulting transfer functions $\widehat{h}(\omega)$ and $\widehat{\bar{g}}(\omega)$ are polynomials in $\mathrm{e}^{-i\omega}$. We suppose that these polynomials have no common zeros. The Bezout Theorem 7.6 on polynomials proves that if $P(z)$ and $Q(z)$ are two polynomials of degree n and l, with no common zeros, then there exists a unique pair of polynomials $\tilde{P}(z)$ and $\tilde{Q}(z)$ of degree $l-1$ and $n-1$ such that

$$P(z)\tilde{P}(z) + Q(z)\tilde{Q}(z) = 1. \tag{5.80}$$

This guarantees the existence of $\widehat{\tilde{h}}(\omega)$ and $\widehat{\tilde{g}}(\omega)$ that are polynomials in $\mathrm{e}^{-i\omega}$ and satisfy (5.78). These are the Fourier transforms of the finite impulse response filters $\tilde{h}$ and $\tilde{g}$. One must however be careful because the resulting scaling function $\widehat{\tilde{\phi}}$ in (5.76) does not necessarily have a finite energy.

Spline Dyadic Wavelets A *box spline* of degree m is a translation of $m+1$ convolutions of $\mathbf{1}_{[0,1]}$ with itself. It is centered at $t=1/2$ if m is even and at $t=0$ if m is odd. Its Fourier transform is

$$\hat{\phi}(\omega) = \left(\frac{\sin(\omega/2)}{\omega/2}\right)^{m+1}\exp\left(\frac{-i\epsilon\omega}{2}\right) \text{ with } \epsilon = \begin{cases}1 & \text{if } m \text{ is even}\\ 0 & \text{if } m \text{ is odd}\end{cases}, \tag{5.81}$$

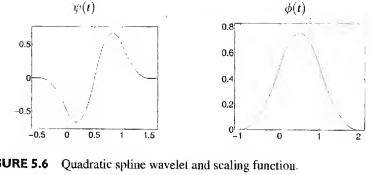

FIGURE 5.6 Quadratic spline wavelet and scaling function.

so

$$\hat{h}(\omega) = \sqrt{2}\,\frac{\hat{\phi}(2\omega)}{\hat{\phi}(\omega)} = \sqrt{2}\left(\cos\frac{\omega}{2}\right)^{m+1}\exp\left(\frac{-i\epsilon\omega}{2}\right). \tag{5.82}$$

We construct a wavelet that has one vanishing moment by choosing $\hat{g}(\omega) = O(\omega)$ in the neighborhood of $\omega=0$. For example

$$\hat{g}(\omega) = -i\sqrt{2}\sin\frac{\omega}{2}\exp\left(\frac{-i\epsilon\omega}{2}\right). \tag{5.83}$$

The Fourier transform of the resulting wavelet is

$$\hat{\psi}(\omega) = \frac{1}{\sqrt{2}}\hat{g}\left(\frac{\omega}{2}\right)\hat{\phi}\left(\frac{\omega}{2}\right) = \frac{-i\omega}{4}\left(\frac{\sin(\omega/4)}{\omega/4}\right)^{m+2}\exp\left(\frac{-i\omega(1+\epsilon)}{4}\right). \tag{5.84}$$

It is the first derivative of a box spline of degree $m+1$ centered at $t=(1+\epsilon)/4$. For $m=2$, Figure 5.6 shows the resulting quadratic splines ϕ and ψ. The dyadic admissibility condition (5.68) is verified numerically for $A=0.505$ and $B=0.522$.

To design dual scaling functions $\tilde{\phi}$ and wavelets $\tilde{\psi}$ which are splines, we choose $\widehat{\tilde{h}} = \hat{h}$. As a consequence, $\phi=\tilde{\phi}$ and the reconstruction condition (5.78) implies that

$$\widehat{\tilde{g}}(\omega) = \frac{2-|\hat{h}(\omega)|^2}{\hat{g}^*(\omega)} = -i\sqrt{2}\exp\left(\frac{-i\omega}{2}\right)\sin\frac{\omega}{2}\sum_{n=0}^{m}\left(\cos\frac{\omega}{2}\right)^{2n}. \tag{5.85}$$

Table 5.3 gives the corresponding filters for $m=2$.

5.5.2 "Algorithme à Trous"

Suppose that the scaling functions and wavelets ϕ, ψ, $\tilde{\phi}$ and $\tilde{\psi}$ are designed with the filters h, g, $\tilde{h}$ and $\tilde{g}$. A fast dyadic wavelet transform is calculated with a filter bank algorithm called in French the *algorithme à trous*, introduced by Holschneider, Kronland-Martinet, Morlet and Tchamitchian [212]. It is similar to a fast biorthogonal wavelet transform, without subsampling [308, 261].

n	$h[n]/\sqrt{2}$	$\tilde{h}[n]/\sqrt{2}$	$g[n]/\sqrt{2}$	$\tilde{g}[n]/\sqrt{2}$
−2				−0.03125
−1	0.125	0.125		−0.21875
0	0.375	0.375	−0.5	−0.6875
1	0.375	0.375	0.5	0.6875
2	0.125	0.125		0.21875
3				0.03125

Table 5.3 Coefficients of the filters computed from their transfer functions (5.82, 5.83, 5.85) for $m = 2$. These filters generate the quadratic spline scaling functions and wavelets shown in Figure 5.6.

Let $\bar{f}(t)$ be a continuous time signal characterized by N samples at a distance N^{-1} over $[0,1]$. Its dyadic wavelet transform can only be calculated at scales $1 > 2^J \geq N^{-1}$. To simplify the description of the filter bank algorithm, it is easier to consider the signal $f(t) = \bar{f}(N^{-1}t)$, whose samples have distance equal to 1. A change of variable in the dyadic wavelet transform integral shows that $Wf(u,2^j) = N^{-1/2}Wf(Nu,N2^j)$. We thus concentrate on the dyadic wavelet transform of f, from which the dyadic wavelet transform of $\bar{f}$ is easily derived.

Fast Dyadic Transform We suppose that the samples $a_0[n]$ of the input discrete signal are not equal to $f(n)$ but to a local average of f in the neighborhood of $t = n$. Indeed, the detectors of signal acquisition devices perform such an averaging. The samples $a_0[n]$ are written as averages of $f(t)$ weighted by the scaling kernels $\phi(t-n)$:

$$a_0[n] = \langle f(t), \phi(t-n)\rangle = \int_{-\infty}^{+\infty} f(t)\,\phi(t-n)\,dt.$$

This is further justified in Section 7.3.1. For any $j \geq 0$, we denote

$$a_j[n] = \langle f(t), \phi_{2^j}(t-n)\rangle \quad \text{with} \quad \phi_{2^j}(t) = \frac{1}{\sqrt{2^j}}\phi\Big(\frac{t}{2^j}\Big).$$

The dyadic wavelet coefficients are computed for $j > 0$ over the integer grid

$$d_j[n] = Wf(n,2^j) = \langle f(t), \psi_{2^j}(t-n)\rangle.$$

For any filter $x[n]$, we denote by $x_j[n]$ the filters obtained by inserting $2^j - 1$ zeros between each sample of $x[n]$. Its Fourier transform is $\hat{x}(2^j\omega)$. Inserting zeros in the filters creates holes (*trous* in French). Let $\bar{x}_j[n] = x_j[-n]$. The next proposition gives convolution formulas that are cascaded to compute a dyadic wavelet transform and its inverse.

Proposition 5.6 *For any $j \geq 0$,*

$$a_{j+1}[n] = a_j \star \bar{h}_j[n] \quad , \quad d_{j+1}[n] = a_j \star \bar{g}_j[n] \ , \tag{5.86}$$

and

$$a_j[n] = \frac{1}{2}\left(a_{j+1} \star \tilde{h}_j[n] + d_{j+1} \star \tilde{g}_j[n]\right). \tag{5.87}$$

Proof[2]. *Proof of (5.86).* Since

$$a_{j+1}[n] = f \star \bar{\phi}_{2^{j+1}}(n) \quad \text{and} \quad d_{j+1}[n] = f \star \bar{\psi}_{2^{j+1}}(n),$$

we verify with (3.3) that their Fourier transforms are respectively

$$\hat{a}_{j+1}(\omega) = \sum_{k=-\infty}^{+\infty} \hat{f}(\omega + 2k\pi)\,\hat{\phi}^*_{2^{j+1}}(\omega + 2k\pi)$$

and

$$\hat{d}_{j+1}(\omega) = \sum_{k=-\infty}^{+\infty} \hat{f}(\omega + 2k\pi)\,\hat{\psi}^*_{2^{j+1}}(\omega + 2k\pi).$$

The properties (5.76) and (5.77) imply that

$$\hat{\phi}_{2^{j+1}}(\omega) = \sqrt{2^{j+1}}\,\hat{\phi}(2^{j+1}\omega) = \hat{h}(2^j\omega)\sqrt{2^j}\,\hat{\phi}(2^j\omega),$$

$$\hat{\psi}_{2^{j+1}}(\omega) = \sqrt{2^{j+1}}\,\hat{\psi}(2^{j+1}\omega) = \hat{g}(2^j\omega)\sqrt{2^j}\,\hat{\phi}(2^j\omega).$$

Since $j \geq 0$, both $\hat{h}(2^j\omega)$ and $\hat{g}(2^j\omega)$ are 2π periodic, so

$$\hat{a}_{j+1}(\omega) = \hat{h}^*(2^j\omega)\,\hat{a}_j(\omega) \ \text{ and } \ \hat{d}_{j+1}(\omega) = \hat{g}^*(2^j\omega)\,\hat{a}_j(\omega). \tag{5.88}$$

These two equations are the Fourier transforms of (5.86).

Proof of (5.87). Equations (5.88) imply

$$\hat{a}_{j+1}(\omega)\,\hat{\tilde{h}}(2^j\omega) + \hat{d}_{j+1}(\omega)\,\hat{\tilde{g}}(2^j\omega) = \hat{a}_j(\omega)\,\hat{h}^*(2^j\omega)\,\hat{\tilde{h}}(2^j\omega) + \hat{a}_j(\omega)\,\hat{g}^*(2^j\omega)\,\hat{\tilde{g}}(2^j\omega).$$

Inserting the reconstruction condition (5.78) proves that

$$\hat{a}_{j+1}(\omega)\,\hat{\tilde{h}}(2^j\omega) + \hat{d}_{j+1}(\omega)\,\hat{\tilde{g}}(2^j\omega) = 2\hat{a}_j(\omega),$$

which is the Fourier transform of (5.87). ∎

The dyadic wavelet representation of a_0 is defined as the set of wavelet coefficients up to a scale 2^J plus the remaining low-frequency information a_J:

$$\left[\{d_j\}_{1\leq j\leq J}\,,\ a_J\right]. \tag{5.89}$$

It is computed from a_0 by cascading the convolutions (5.86) for $0 \leq j < J$, as illustrated in Figure 5.7(a). The dyadic wavelet transform of Figure 5.5 is calculated with this filter bank algorithm. The original signal a_0 is recovered from its wavelet representation (5.89) by iterating (5.87) for $J > j \geq 0$, as illustrated in Figure 5.7(b).

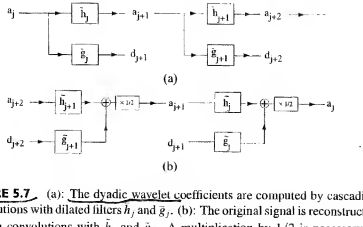

FIGURE 5.7. (a): The dyadic wavelet coefficients are computed by cascading convolutions with dilated filters $\bar{h}_j$ and $\bar{g}_j$. (b): The original signal is reconstructed through convolutions with $\tilde{h}_j$ and $\tilde{g}_j$. A multiplication by $1/2$ is necessary to recover the next finer scale signal a_j.

If the input signal $a_0[n]$ has a finite size of N samples, the convolutions (5.86) are replaced by circular convolutions. The maximum scale 2^J is then limited to N, and for $J = \log_2 N$ one can verify that $a_J[n]$ is constant and equal to $N^{-1/2}\sum_{n=0}^{N-1} a_0[n]$. Suppose that h and g have respectively K_h and K_g non-zero samples. The "dilated" filters h_j and g_j have the same number of non-zero coefficients. The number of multiplications needed to compute a_{j+1} and d_{j+1} from a_j or the reverse is thus equal to $(K_h + K_g)N$. For $J = \log_2 N$, the dyadic wavelet representation (5.89) and its inverse are thus calculated with $(K_h + K_g)N\log_2 N$ multiplications and additions.

5.5.3 Oriented Wavelets for a Vision [3]

Image processing applications of dyadic wavelet transforms are motivated by many physiological and computer vision studies. Textures can be synthesized and discriminated with oriented two-dimensional wavelet transforms. Section 6.3 relates multiscale edges to the local maxima of a wavelet transform.

Oriented Wavelets In two dimensions, a dyadic wavelet transform is computed with several mother wavelets $\{\psi^k\}_{1\le k\le K}$ which often have different spatial orientations. For $x = (x_1, x_2)$, we denote

$$\psi^k_{2^j}(x_1,x_2) = \frac{1}{2^j}\,\psi^k\left(\frac{x_1}{2^j},\frac{x_2}{2^j}\right) \quad \text{and} \quad \bar{\psi}^k_{2^j}(x) = \psi^k_{2^j}(-x).$$

The wavelet transform of $f \in \mathbf{L}^2(\mathbb{R}^2)$ in the direction k is defined at the position $u = (u_1, u_2)$ and at the scale 2^j by

$$W^k f(u,2^j) = f(v)\,\psi^k_{2^j}(v-u)\big|_{v=u} = f \star \bar{\psi}^k_{2^j}(u) \tag{5.90}$$

As in Theorem 5.11, one can prove that the two-dimensional wavelet transform is a complete and stable signal representation if there exist $A > 0$ and B such that

$$\forall \omega = (\omega_1,\omega_2) \in \mathbb{R}^2 - \{(0,0)\}\ ,\ A \le \sum_{k=1}^{K}\sum_{j=-\infty}^{+\infty} |\hat{\psi}^k(2^j\omega)|^2 \le B. \tag{5.91}$$

Then there exist reconstruction wavelets $\{\tilde{\psi}^k\}_{1\le k\le K}$ whose Fourier transforms satisfy

$$\sum_{j=-\infty}^{+\infty} \frac{1}{2^{2j}} \sum_{k=1}^{K} \widehat{\tilde{\psi}^k}(2^j\omega)\,\hat{\psi}^{k*}(2^j\omega) = 1\,, \tag{5.92}$$

which yields

$$f(x) = \sum_{j=-\infty}^{+\infty} \frac{1}{2^{2j}} \sum_{k=1}^{K} W^k f(.,2^j) \star \bar{\tilde{\psi}}^k_{2^j}(x)\,. \tag{5.93}$$

Wavelets that satisfy (5.91) are called *dyadic wavelets*.

Families of oriented wavelets along any angle α can be designed as a linear expansion of K mother wavelets [312]. For example, a wavelet in the direction α may be defined as the partial derivative of order p of a window $\theta(x)$ in the direction of the vector $\vec{n} = (\cos\alpha, \sin\alpha)$:

$$\psi^\alpha(x) = \frac{\partial^p \theta(x)}{\partial \vec{n}^p} = \left(\cos\alpha\,\frac{\partial}{\partial x_1} + \sin\alpha\,\frac{\partial}{\partial x_2}\right)^p \theta(x).$$

This partial derivative is a linear expansion of $K = p+1$ mother wavelets

$$\psi^\alpha(x) = \sum_{k=0}^{p} \binom{p}{k} (\cos\alpha)^k (\sin\alpha)^{p-k}\,\psi^k(x)\,, \tag{5.94}$$

with

$$\psi^k(x) = \frac{\partial^p \theta(x)}{\partial x_1^k\,\partial x_2^{p-k}} \quad \text{for } 0 \le k \le p.$$

For appropriate windows θ, these $p+1$ partial derivatives define a family of dyadic wavelets. In the direction α, the wavelet transform $W^\alpha f(u,2^j) = f \star \bar{\psi}^\alpha_{2^j}(u)$ is computed from the $p+1$ components $W^k f(u,2^j) = f \star \bar{\psi}^k_{2^j}(u)$ with the expansion (5.94). Section 6.3 uses such oriented wavelets, with $p = 1$, to detect the multiscale edges of an image.

Gabor Wavelets In the cat's visual cortex, Hubel and Wiesel [215] discovered a class of cells, called simple cells, whose responses depend on the frequency and orientation of the visual stimuli. Numerous physiological experiments [283] have shown that these cells can be modeled as linear filters, whose impulse responses have been measured at different locations of the visual cortex. Daugman [149]

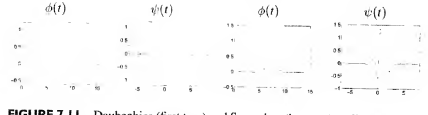

FIGURE 7.11 Daubechies (first two) and Symmlets (last two) scaling functions and wavelets with $p = 8$ vanishing moments.

Coiflets For an application in numerical analysis, Coifman asked Daubechies [144] to construct a family of wavelets ψ that have p vanishing moments and a minimum size support, but whose scaling functions also satisfy

$$\int_{-\infty}^{+\infty} \phi(t)\,dt = 1 \quad \text{and} \quad \int_{-\infty}^{+\infty} t^k \phi(t)\,dt = 0 \quad \text{for } 1 \le k < p. \tag{7.104}$$

Such scaling functions are useful in establishing precise quadrature formulas. If f is $\mathbf{C}^k$ in the neighborhood of $2^J n$ with $k < p$, then a Taylor expansion of f up to order k shows that

$$2^{-J/2}\langle f, \phi_{J,n}\rangle \approx f(2^J n) + O(2^{(k+1)J}). \tag{7.105}$$

At a fine scale 2^J, the scaling coefficients are thus closely approximated by the signal samples. The order of approximation increases with p. The supplementary condition (7.104) requires increasing the support of ψ; the resulting Coiflet has a support of size $3p-1$ instead of $2p-1$ for a Daubechies wavclet. The corresponding conjugate mirror filters are tabulated in WAVELAB.

Audio Filters The first conjugate mirror filters with finite impulse response were constructed in 1986 by Smith and Barnwell [317] in the context of perfect filter bank reconstruction, explained in Section 7.3.2. These filters satisfy the quadrature condition $|\hat{h}(\omega)|^2 + |\hat{h}(\omega+\pi)|^2 = 2$, which is necessary and sufficient for filter bank reconstruction. However, $\hat{h}(0) \neq \sqrt{2}$ so the infinite product of such filters does not yield a wavelet basis of $\mathbf{L}^2(\mathbb{R})$. Instead of imposing any vanishing moments, Smith and Barnwell [317], and later Vaidyanathan and Hoang [337], designed their filters to reduce the size of the transition band. where $|\hat{h}(\omega)|$ decays from nearly $\sqrt{2}$ to nearly 0 in the neighborhood of $\pm\pi/2$. This constraint is important in optimizing the transform code of audio signals, explained in Section 11.3.3. However, many cascades of these filters exhibit wild behavior. The Vaidyanathan-Hoang filters are tabulated in WAVELAB. Many other classes of conjugate mirror filters with finite impulse response have been constructed [74, 73]. Recursive conjugate mirror filters may also be designed [209] to minimize the size of the transition band for a given number of zeros at $\omega = \pi$. These filters have a fast but non-causal recursive implementation for signals of finite size.

7.3 WAVELETS AND FILTER BANKS [1]

Decomposition coefficients in a wavelet orthogonal basis are computed with a fast algorithm that cascades discrete convolutions with h and g, and subsamples the output. Section 7.3.1 derives this result from the embedded structure of multiresolution approximations. A direct filter bank analysis is performed in Section 7.3.2, which gives more general perfect reconstruction conditions on the filters. Section 7.3.3 shows that perfect reconstruction filter banks decompose signals in a basis of $\mathbf{l}^2(\mathbb{Z})$. This basis is orthogonal for conjugate mirror filters.

7.3.1 Fast Orthogonal Wavelet Transform

We describe a fast filter bank algorithm that computes the orthogonal wavelet coefficients of a signal measured at a finite resolution. A fast wavelet transform decomposes successively each approximation $P_{\mathbf{V}_j} f$ into a coarser approximation $P_{\mathbf{V}_{j+1}} f$ plus the wavelet coefficients carried by $P_{\mathbf{W}_{j+1}} f$. In the other direction, the reconstruction from wavelet coefficients recovers each $P_{\mathbf{V}_j} f$ from $P_{\mathbf{V}_{j+1}} f$ and $P_{\mathbf{W}_{j+1}} f$.

Since $\{\phi_{j,n}\}_{n\in\mathbb{Z}}$ and $\{\psi_{j,n}\}_{n\in\mathbb{Z}}$ are orthonormal bases of $\mathbf{V}_j$ and $\mathbf{W}_j$ the projection in these spaces is characterized by

$$a_j[n] = \langle f, \phi_{j,n}\rangle \text{ and } d_j[n] = \langle f, \psi_{j,n}\rangle .$$

The following theorem [253, 255] shows that these coefficients are calculated with a cascade of discrete convolutions and subsamplings. We denote $\bar{x}[n] = x[-n]$ and

$$\check{x}[n] = \begin{cases} x[p] & \text{if } n = 2p \\ 0 & \text{if } n = 2p+1 \end{cases}. \tag{7.106}$$

Theorem 7.7 (MALLAT) *At the decomposition*

$$a_{j+1}[p] = \sum_{n=-\infty}^{+\infty} h[n-2p]\,a_j[n] = a_j \star \bar{h}[2p], \tag{7.107}$$

$$d_{j+1}[p] = \sum_{n=-\infty}^{+\infty} g[n-2p]\,a_j[n] = a_j \star \bar{g}[2p]. \tag{7.108}$$

At the reconstruction,

$$\begin{aligned} a_j[p] &= \sum_{n=-\infty}^{+\infty} h[p-2n]\,a_{j+1}[n] + \sum_{n=-\infty}^{+\infty} g[p-2n]\,d_{j+1}[n] \\ &= \check{a}_{j+1} \star h[p] + \check{d}_{j+1} \star g[p]. \end{aligned} \tag{7.109}$$

Proof [1]. *Proof of (7.107)* Any $\phi_{j+1,p} \in \mathbf{V}_{j+1} \subset \mathbf{V}_j$ can be decomposed in the orthonormal basis $\{\phi_{j,n}\}_{n\in\mathbb{Z}}$ of $\mathbf{V}_j$:

$$\phi_{j+1,p} = \sum_{n=-\infty}^{+\infty} \langle \phi_{j+1,p}, \phi_{j,n}\rangle\, \phi_{j,n}. \tag{7.110}$$

With the change of variable $t' = 2^{-j}t - 2p$ we obtain

$$\begin{aligned}\langle \phi_{j+1,p}, \phi_{j,n}\rangle &= \int_{-\infty}^{+\infty} \frac{1}{\sqrt{2^{j+1}}}\phi\left(\frac{t-2^{j+1}p}{2^{j+1}}\right)\frac{1}{\sqrt{2^j}}\phi^*\left(\frac{t-2^j n}{2^j}\right)dt \\ &= \int_{-\infty}^{+\infty} \frac{1}{\sqrt{2}}\phi\left(\frac{t}{2}\right)\phi^*(t-n+2p)dt \\ &= \left\langle \frac{1}{\sqrt{2}}\phi\left(\frac{t}{2}\right), \phi(t-n+2p)\right\rangle = h[n-2p]. \end{aligned} \tag{7.111}$$

Hence (7.110) implies that

$$\phi_{j+1,p} = \sum_{n=-\infty}^{+\infty} h[n-2p]\,\phi_{j,n}. \tag{7.112}$$

Computing the inner product of f with the vectors on each side of this equality yields (7.107).

Proof of (7.108) Since $\psi_{j+1,p} \in \mathbf{W}_{j+1} \subset \mathbf{V}_j$, it can be decomposed as

$$\psi_{j+1,p} = \sum_{n=-\infty}^{+\infty} \langle \psi_{j+1,p}, \phi_{j,n}\rangle\, \phi_{j,n}.$$

As in (7.111), the change of variable $t' = 2^{-j}t - 2p$ proves that

$$\langle \psi_{j+1,p}, \phi_{j,n}\rangle = \left\langle \frac{1}{\sqrt{2}}\psi\left(\frac{t}{2}\right), \phi(t-n+2p)\right\rangle = g[n-2p] \tag{7.113}$$

and hence

$$\psi_{j+1,p} = \sum_{n=-\infty}^{+\infty} g[n-2p]\,\phi_{j,n}. \tag{7.114}$$

Taking the inner product with f on each side gives (7.108).

Proof of (7.109) Since $\mathbf{W}_{j+1}$ is the orthogonal complement of $\mathbf{V}_{j+1}$ in $\mathbf{V}_j$ the union of the two bases $\{\psi_{j+1,n}\}_{n\in\mathbb{Z}}$ and $\{\phi_{j+1,n}\}_{n\in\mathbb{Z}}$ is an orthonormal basis of $\mathbf{V}_j$. Hence any $\phi_{j,p}$ can be decomposed in this basis:

$$\begin{aligned}\phi_{j,p} &= \sum_{n=-\infty}^{+\infty} \langle \phi_{j,p}, \phi_{j+1,n}\rangle \phi_{j+1,n} \\ &\quad + \sum_{n=-\infty}^{+\infty} \langle \phi_{j,p}, \psi_{j+1,n}\rangle \psi_{j+1,n}.\end{aligned}$$

Inserting (7.111) and (7.113) yields

$$\phi_{j,p} = \sum_{n=-\infty}^{+\infty} h[p-2n]\,\phi_{j+1,n} + \sum_{n=-\infty}^{+\infty} g[p-2n]\,\psi_{j+1,n}.$$

Taking the inner product with f on both sides of this equality gives (7.109) ■

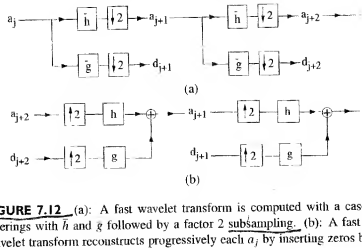

FIGURE 7.12 (a): A fast wavelet transform is computed with a cascade of filterings with $\bar{h}$ and $\bar{g}$ followed by a factor 2 subsampling. (b): A fast inverse wavelet transform reconstructs progressively each a_j by inserting zeros between samples of a_{j+1} and d_{j+1}, filtering and adding the output.

Theorem 7.7 proves that a_{j+1} and d_{j+1} are computed by taking every other sample of the convolution of a_j with h and $\bar{g}$ respectively, as illustrated by Figure 7.12. The filter $\bar{h}$ removes the higher frequencies of the inner product sequence a_j whereas $\bar{g}$ is a high-pass filter which collects the remaining highest frequencies. The reconstruction (7.109) is an interpolation that inserts zeros to expand a_{j+1} and d_{j+1} and filters these signals, as shown in Figure 7.12.

An *orthogonal wavelet representation* of $a_L = \langle f, \phi_{L,n}\rangle$ is composed of wavelet coefficients of f at scales $2^L < 2^j \leq 2^J$ plus the remaining approximation at the largest scale 2^J:

$$\{\{d_j\}_{L<j\leq J},\ a_J\}. \tag{7.115}$$

It is computed from a_L by iterating (7.107) and (7.108) for $L < j \leq J$. Figure 7.7 gives a numerical example computed with the cubic spline filter of Table 7.1. The original signal a_L is recovered from this wavelet representation by iterating the reconstruction (7.109) for $J > j \geq L$.

Initialization Most often the discrete input signal $b[n]$ is obtained by a finite resolution device that averages and samples an analog input signal. For example, a CCD camera filters the light intensity by the optics and each photo-receptor averages the input light over its support. A pixel value thus measures average light intensity. If the sampling distance is N^{-1}, to define and compute the wavelet coefficients, we need to associate to $b[n]$ a function $f(t) \in \mathbf{V}_L$ approximated at the scale $2^L = N^{-1}$, and compute $a_L[n] = \langle f, \phi_{L,n}\rangle$. Problem 7.6 explains how to compute $a_L[n] = \langle f, \phi_{L,n}\rangle$ so that $b[n] = f(N^{-1}n)$.

A simpler and faster approach considers

$$f(t) = \sum_{n=-\infty}^{+\infty} b[n]\,\phi\left(\frac{t-2^L n}{2^L}\right) \in \mathbf{V}_L .$$

Since $\{\phi_{L,n}(t) = 2^{-L/2}\phi(2^{-L}t - n)\}_{n\in\mathbb{Z}}$ is orthonormal and $2^L = N^{-1}$,

$$b[n] = N^{1/2}\langle f, \phi_{L,n}\rangle = N^{1/2}\,a_L[n] .$$

But $\int_{-\infty}^{\infty}\phi(t)\,dt = 1$, so

$$N^{1/2}a_L[n] = \int_{-\infty}^{+\infty} f(t)\,\frac{1}{N^{-1}}\,\phi\left(\frac{t-N^{-1}n}{N^{-1}}\right)dt$$

is a weighted average of f in the neighborhood of $N^{-1}n$ over a domain proportional to N^{-1}. Hence if f is regular,

$$b[n] = N^{1/2}\,a_L[n] \approx f(N^{-1}n) . \tag{7.116}$$

If ψ is a Coiflet and $f(t)$ is regular in the neighborhood of $N^{-1}n$, then (7.105) shows that $N^{-1/2}a_L[n]$ is a high order approximation of $f(N^{-1}n)$.

Finite Signals Let us consider a signal f whose support is in $[0,1]$ and which is approximated with a uniform sampling at intervals N^{-1}. The resulting approximation a_L has $N = 2^{-L}$ samples. This is the case in Figure 7.7 with $N = 1024$. Computing the convolutions with $\bar{h}$ and $\bar{g}$ at abscissa close to 0 or close to N requires knowing the values of $a_L[n]$ beyond the boundaries $n = 0$ and $n = N-1$. These boundary problems may be solved with one of the three approaches described in Section 7.5.

Section 7.5.1 explains the simplest algorithm, which periodizes a_L. The convolutions in Theorem 7.7 are replaced by circular convolutions. This is equivalent to decomposing f in a periodic wavelet basis of $\mathbf{L}^2[0,1]$. This algorithm has the disadvantage of creating large wavelet coefficients at the borders.

If ψ is symmetric or antisymmetric, we can use a folding procedure described in Section 7.5.2, which creates smaller wavelet coefficients at the border. It decomposes f in a folded wavelet basis of $\mathbf{L}^2[0,1]$. However, we mentioned in Section 7.2.3 that Haar is the only symmetric wavelet with a compact support. Higher order spline wavelets have a symmetry but h must be truncated in numerical calculations.

The most efficient boundary treatment is described in Section 7.5.3, but the implementation is more complicated. Boundary wavelets which keep their vanishing moments are designed to avoid creating large amplitude coefficients when f is regular. The fast algorithm is implemented with special boundary filters, and requires the same number of calculations as the two other methods.

Complexity Suppose that h and g have K non-zero coefficients. Let a_L be a signal of size $N = 2^{-L}$. With appropriate boundary calculations, each a_j and d_j has 2^{-j} samples. Equations (7.107) and (7.108) compute a_{j+1} and d_{j+1} from a_j with $2^{-j}K$ additions and multiplications. The wavelet representation (7.115) is therefore calculated with at most $2KN$ additions and multiplications. The reconstruction (7.109) of a_j from a_{j+1} and d_{j+1} is also obtained with $2^{-j}K$ additions and multiplications. The original signal a_L is thus also recovered from the wavelet representation with at most $2KN$ additions and multiplications.

Wavelet Graphs The graphs of ϕ and ψ are computed numerically with the inverse wavelet transform. If $f = \phi$ then $a_0[n] = \delta[n]$ and $d_j[n] = 0$ for all $L < j \leq 0$. The inverse wavelet transform computes a_L and (7.116) shows that

$$N^{1/2}a_L[n] \approx \phi(N^{-1}n) .$$

If ϕ is regular and N is large enough, we recover a precise approximation of the graph of ϕ from a_L.

Similarly, if $f = \psi$ then $a_0[n] = 0$, $d_0[n] = \delta[n]$ and $d_j[n] = 0$ for $L < j < 0$. Then $a_L[n]$ is calculated with the inverse wavelet transform and $N^{1/2}a_L[n] \approx \psi(N^{-1}n)$. The Daubechies wavelets and scaling functions in Figure 7.10 are calculated with this procedure.

7.3.2 Perfect Reconstruction Filter Banks

The fast discrete wavelet transform decomposes signals into low-pass and high-pass components subsampled by 2; the inverse transform performs the reconstruction. The study of such classical multirate filter banks became a major signal processing topic in 1976, when Croisier, Esteban and Galand [141] discovered that it is possible to perform such decompositions and reconstructions with *quadrature mirror filters* (Problem 7.7). However, besides the simple Haar filter, a quadrature mirror filter can not have a finite impulse response. In 1984, Smith and Barnwell [316] and Mintzer [272] found necessary and sufficient conditions for obtaining perfect reconstruction orthogonal filters with a finite impulse response, that they called *conjugate mirror filters*. The theory was completed by the biorthogonal equations of Vetterli [338, 339] and the general paraunitary matrix theory of Vaidyanathan [336]. We follow this digital signal processing approach which gives a simple understanding of conjugate mirror filter conditions. More complete presentations of filter banks properties can be found in [1, 2, 68, 73, 74].

Filter Bank A two-channel multirate filter bank convolves a signal a_0 with a low-pass filter $\bar{h}[n] = h[-n]$ and a high-pass filter $\bar{g}[n] = g[-n]$ and subsamples by 2 the output:

$$a_1[n] = a_0 \star \bar{h}[2n] \text{ and } d_1[n] = a_0 \star \bar{g}[2n]. \tag{7.117}$$

A reconstructed signal $\tilde{a}_0$ is obtained by filtering the zero expanded signals with a dual low-pass filter $\tilde{h}$ and a dual high-pass filter $\tilde{g}$, as shown in Figure 7.13. With

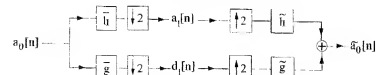

FIGURE 7.13 The input signal is filtered by a low-pass and a high-pass filter and subsampled. The reconstruction is performed by inserting zeros and filtering with dual filters $\tilde{h}$ and $\tilde{g}$.

the zero insertion notation (7.106) it yields

$$\tilde{a}_0[n] = \tilde{a}_1 \star \tilde{h}[n] + \tilde{d}_1 \star \tilde{g}[n]. \tag{7.118}$$

We study necessary and sufficient conditions on h, g, $\tilde{h}$ and $\tilde{g}$ to guarantee a perfect reconstruction $\tilde{a}_0 = a_0$.

Subsampling and Zero Interpolation Subsamplings and expansions with zero insertions have simple expressions in the Fourier domain. Since $\hat{x}(\omega) = \sum_{n=-\infty}^{+\infty} x[n]\, e^{-in\omega}$ the Fourier series of the subsampled signal $y[n] = x[2n]$ can be written

$$\hat{y}(2\omega) = \sum_{n=-\infty}^{+\infty} x[2n]\, e^{-i2n\omega} = \frac{1}{2}\left(\hat{x}(\omega) + \hat{x}(\omega+\pi)\right). \tag{7.119}$$

The component $\hat{x}(\omega+\pi)$ creates a frequency folding. This *aliasing* must be canceled at the reconstruction.

The insertion of zeros defines

$$y[n] = \check{x}[n] = \begin{cases} x[p] & \text{if } n = 2p \\ 0 & \text{if } n = 2p+1 \end{cases}$$

whose Fourier transform is

$$\hat{y}(\omega) = \sum_{n=-\infty}^{+\infty} x[n]\, e^{-i2n\omega} = \hat{x}(2\omega). \tag{7.120}$$

The following theorem gives Vetterli's [339] biorthogonal conditions, which guarantee that $\tilde{a}_0 = a_0$.

Theorem 7.8 (VETTERLI) *The filter bank performs an exact reconstruction for any input signal if and only if*

$$\hat{h}^*(\omega+\pi)\,\hat{\tilde{h}}(\omega) + \hat{g}^*(\omega+\pi)\,\hat{\tilde{g}}(\omega) = 0, \tag{7.121}$$

and

$$\hat{h}^*(\omega)\,\hat{\tilde{h}}(\omega) + \hat{g}^*(\omega)\,\hat{\tilde{g}}(\omega) = 2. \tag{7.122}$$

Proof [1]. We first relate the Fourier transform of a_1 and d_1 to the Fourier transform of a_0. Since h and g are real, the transfer functions of h and g are respectively $\hat{h}(-\omega) = \hat{h}^*(\omega)$ and $\hat{g}(-\omega) = \hat{g}^*(\omega)$. By using (7.119), we derive from the definition (7.117) of a_1 and d_1 that

$$\hat{a}_1(2\omega) = \frac{1}{2}\left(\hat{a}_0(\omega)\,\hat{h}^*(\omega) + \hat{a}_0(\omega+\pi)\,\hat{h}^*(\omega+\pi)\right), \tag{7.123}$$

$$\hat{d}_1(2\omega) = \frac{1}{2}\left(\hat{a}_0(\omega)\,\hat{g}^*(\omega) + \hat{a}_0(\omega+\pi)\,\hat{g}^*(\omega+\pi)\right). \tag{7.124}$$

The expression (7.118) of $\tilde{a}_0$ and the zero insertion property (7.120) also imply

$$\hat{\tilde{a}}_0(\omega) = \hat{\tilde{a}}_1(2\omega)\,\hat{\tilde{h}}(\omega) + \hat{d}_1(2\omega)\,\hat{\tilde{g}}(\omega). \tag{7.125}$$

Hence

$$\hat{\tilde{a}}_0(\omega) = \frac{1}{2}\left(\hat{h}^*(\omega)\hat{\tilde{h}}(\omega) + \hat{g}^*(\omega)\hat{\tilde{g}}(\omega)\right)\hat{a}_0(\omega) + \frac{1}{2}\left(\hat{h}^*(\omega+\pi)\hat{\tilde{h}}(\omega) + \hat{g}^*(\omega+\pi)\hat{\tilde{g}}(\omega)\right)\hat{a}_0(\omega+\pi).$$

To obtain $a_0 = \tilde{a}_0$ for all a_0, the filters must cancel the aliasing term $\hat{a}_0(\omega+\pi)$ and guarantee a unit gain for $\hat{a}_0(\omega)$, which proves equations (7.121) and (7.122). ■

Theorem 7.8 proves that the reconstruction filters $\tilde{h}$ and $\tilde{g}$ are entirely specified by the decomposition filters h and g. In matrix form, it can be rewritten

$$\begin{pmatrix} \hat{h}(\omega) & \hat{g}(\omega) \\ \hat{h}(\omega+\pi) & \hat{g}(\omega+\pi) \end{pmatrix} \times \begin{pmatrix} \hat{\tilde{h}}^*(\omega) \\ \hat{\tilde{g}}^*(\omega) \end{pmatrix} = \begin{pmatrix} 2 \\ 0 \end{pmatrix}. \tag{7.126}$$

The inversion of this 2×2 matrix yields

$$\begin{pmatrix} \hat{\tilde{h}}^*(\omega) \\ \hat{\tilde{g}}^*(\omega) \end{pmatrix} = \frac{2}{\Delta(\omega)} \begin{pmatrix} \hat{g}(\omega+\pi) \\ -\hat{h}(\omega+\pi) \end{pmatrix} \tag{7.127}$$

where $\Delta(\omega)$ is the determinant

$$\Delta(\omega) = \hat{h}(\omega)\,\hat{g}(\omega+\pi) - \hat{h}(\omega+\pi)\,\hat{g}(\omega). \tag{7.128}$$

The reconstruction filters are stable only if the determinant does not vanish for all $\omega \in [-\pi, \pi]$. Vaidyanathan [336] has extended this result to multirate filter banks with an arbitrary number M of channels by showing that the resulting matrices of filters satisfy paraunitary properties [73].

Finite Impulse Response When all filters have a finite impulse response, the determinant $\Delta(\omega)$ can be evaluated. This yields simpler relations between the decomposition and reconstruction filters.

Theorem 7.9 *Perfect reconstruction filters satisfy*

$$\hat{h}^*(\omega)\hat{\bar{h}}(\omega)+\hat{h}^*(\omega+\pi)\hat{\bar{h}}(\omega+\pi)=2. \tag{7.129}$$

For finite impulse response filters, there exist $a\in\mathbb{R}$ and $l\in\mathbb{Z}$ such that

$$\hat{g}(\omega)=a\,\mathrm{e}^{-i(2l+1)\omega}\hat{\bar{h}}^*(\omega+\pi) \quad\text{and}\quad \hat{\bar{g}}(\omega)=a^{-1}\,\mathrm{e}^{-i(2l+1)\omega}\hat{h}^*(\omega+\pi). \tag{7.130}$$

Proof[1]. Equation (7.127) proves that

$$\hat{\bar{h}}^*(\omega)=\frac{2}{\Delta(\omega)}\hat{g}(\omega+\pi) \quad\text{and}\quad \hat{\bar{g}}^*(\omega)=\frac{-2}{\Delta(\omega)}\hat{h}(\omega+\pi). \tag{7.131}$$

Hence

$$\hat{g}(\omega)\hat{\bar{g}}^*(\omega)=-\frac{\Delta(\omega+\pi)}{\Delta(\omega)}\hat{\bar{h}}^*(\omega+\pi)\hat{h}(\omega+\pi). \tag{7.132}$$

The definition (7.128) implies that $\Delta(\omega+\pi)=-\Delta(\omega)$. Inserting (7.132) in (7.122) yields (7.129).

The Fourier transform of finite impulse response filters is a finite series in $\exp(\pm in\omega)$. The determinant $\Delta(\omega)$ defined by (7.128) is therefore a finite series. Moreover (7.131) proves that $\Delta^{-1}(\omega)$ must also be a finite series. A finite series in $\exp(\pm in\omega)$ whose inverse is also a finite series must have a single term. Since $\Delta(\omega)=-\Delta(\omega+\pi)$ the exponent n must be odd. This proves that there exist $l\in\mathbb{Z}$ and $a\in\mathbb{R}$ such that

$$\Delta(\omega)=-2a\exp[i(2l+1)\omega]. \tag{7.133}$$

Inserting this expression in (7.131) yields (7.130). ∎

The factor a is a gain which is inverse for the decomposition and reconstruction filters and l is a reverse shift. We generally set $a=1$ and $l=0$. In the time domain (7.130) can then be rewritten

$$g[n]=(-1)^{1-n}\bar{h}[1-n] \quad\text{and}\quad \bar{g}[n]=(-1)^{1-n}h[1-n]. \tag{7.134}$$

The two pairs of filters (h,g) and $(\bar{h},\bar{g})$ play a symmetric role and can be inverted.

Conjugate Mirror Filters If we impose that the decomposition filter h is equal to the reconstruction filter $\bar{h}$, then (7.129) is the condition of Smith and Barnwell [316] and Mintzer [272] that defines conjugate mirror filters:

$$|\hat{h}(\omega)|^2+|\hat{h}(\omega+\pi)|^2=2. \tag{7.135}$$

It is identical to the filter condition (7.34) that is required in order to synthesize orthogonal wavelets. The next section proves that it is also equivalent to discrete orthogonality properties.

7.3.3 Biorthogonal Bases of $\mathbf{l}^2(\mathbb{Z})$ [2]

The decomposition of a discrete signal in a multirate filter bank is interpreted as an expansion in a basis of $\mathbf{l}^2(\mathbb{Z})$. Observe first that the low-pass and high-pass signals of a filter bank computed with (7.117) can be rewritten as inner products in $\mathbf{l}^2(\mathbb{Z})$:

$$a_1[l] = \sum_{n=-\infty}^{+\infty} a_0[n]h[n-2l]=\langle a_0[k],h[k-2n]\rangle, \tag{7.136}$$

$$d_1[l] = \sum_{n=-\infty}^{+\infty} a_0[n]g[n-2l]=\langle a_0[n],g[n-2l]\rangle. \tag{7.137}$$

The signal recovered by the reconstructing filters is

$$a_0[n]=\sum_{l=-\infty}^{+\infty} a_1[l]\bar{h}[n-2l]+\sum_{l=-\infty}^{+\infty} d_1[l]\,\bar{g}[n-2l]. \tag{7.138}$$

Inserting (7.136) and (7.137) yields

$$a_0[n]=\sum_{l=-\infty}^{+\infty}\langle f[k],h[k-2l]\rangle\bar{h}[n-2l]+\sum_{l=-\infty}^{+\infty}\langle f[k],g[k-2l]\rangle\bar{g}[n-2l]. \tag{7.139}$$

We recognize the decomposition of a_0 over dual families of vectors $\{\bar{h}[n-2l],\bar{g}[n-2l]\}_{l\in\mathbb{Z}}$ and $\{h[n-2l],g[n-2l]\}_{l\in\mathbb{Z}}$. The following theorem proves that these two families are biorthogonal.

Theorem 7.10 *If h, g, $\bar{h}$ and $\bar{g}$ are perfect reconstruction filters whose Fourier transform is bounded then $\{\bar{h}[n-2l],\bar{g}[n-2l]\}_{l\in\mathbb{Z}}$ and $\{h[n-2l],g[n-2l]\}_{l\in\mathbb{Z}}$ are biorthogonal Riesz bases of $\mathbf{l}^2(\mathbb{Z})$.*

Proof[2]. To prove that these families are biorthogonal we must show that for all $n\in\mathbb{Z}$

$$\langle\bar{h}[n],h[n-2l]\rangle = \delta[l] \tag{7.140}$$

$$\langle\bar{g}[n],g[n-2l]\rangle = \delta[l] \tag{7.141}$$

and

$$\langle\bar{h}[n],g[n-2l]\rangle=\langle\bar{g}[n],h[n-2l]\rangle=0. \tag{7.142}$$

For perfect reconstruction filters, (7.129) proves that

$$\frac{1}{2}\left(\hat{h}^*(\omega)\hat{\bar{h}}(\omega)+\hat{h}^*(\omega+\pi)\hat{\bar{h}}(\omega+\pi)\right)=1.$$

In the time domain, this equation becomes

$$h\star\bar{h}[2l]=\sum_{n=-\infty}^{+\infty}\bar{h}[n]\,h[n-2l]=\delta[l]. \tag{7.143}$$

which verifies (7.140). The same proof as for (7.129) shows that

$$\frac{1}{2}\left(\hat{g}^*(\omega)\,\widehat{\tilde{g}}(\omega)+\hat{g}^*(\omega+\pi)\,\widehat{\tilde{g}}(\omega+\pi)\right)=1.$$

In the time domain, this equation yields (7.141). It also follows from (7.127) that

$$\frac{1}{2}\left(\hat{g}^*(\omega)\,\widehat{\tilde{h}}(\omega)+\hat{g}^*(\omega+\pi)\,\widehat{\tilde{h}}(\omega+\pi)\right)=0,$$

and

$$\frac{1}{2}\left(\hat{h}^*(\omega)\,\widehat{\tilde{g}}(\omega)+\hat{h}^*(\omega+\pi)\,\widehat{\tilde{g}}(\omega+\pi)\right)=0.$$

The inverse Fourier transforms of these two equations yield (7.142).

To finish the proof, one must show the existence of Riesz bounds defined in (A.12). The reader can verify that this is a consequence of the fact that the Fourier transform of each filter is bounded. ■

Orthogonal Bases A Riesz basis is orthonormal if the dual basis is the same as the original basis. For filter banks, this means that $h=\tilde{h}$ and $g=\tilde{g}$. The filter h is then a conjugate mirror filter

$$|\hat{h}(\omega)|^2+|\hat{h}(\omega+\pi)|^2=2. \tag{7.144}$$

The resulting family $\{h[n-2l],g[n-2l]\}_{l\in\mathbb{Z}}$ is an orthogonal basis of $\mathbf{l}^2(\mathbb{Z})$.

Discrete Wavelet Bases The construction of conjugate mirror filters is simpler than the construction of orthogonal wavelet bases of $\mathbf{L}^2(\mathbb{R})$. Why then should we bother with continuous time models of wavelets, since in any case all computations are discrete and rely on conjugate mirror filters? The reason is that conjugate mirror filters are most often used in filter banks that cascade several levels of filterings and subsamplings. It is thus necessary to understand the behavior of such a cascade [290]. In a wavelet filter bank tree, the output of the low-pass filter $\tilde{h}$ is sub-decomposed whereas the output of the high-pass filter $\tilde{g}$ is not; this is illustrated in Figure 7.12. Suppose that the sampling distance of the original discrete signal is N^{-1}. We denote $a_l[n]$ this discrete signal, with $2^L=N^{-1}$. At the depth $j-L\geq 0$ of this filter bank tree, the low-pass signal a_j and high-pass signal d_j can be written

$$a_j[l]=a_L\star\bar{\phi}_j[2^{j-L}l]=\langle a_L[n],\phi_j[n-2^{j-L}l]\rangle$$

and

$$d_j[l]=a_L\star\bar{\psi}_j[2^{j-L}l]=\langle a_L[n],\psi_j[n-2^{j-L}l]\rangle.$$

The Fourier transforms of these equivalent filters are

$$\hat{\phi}_j(\omega)=\prod_{p=0}^{j-L-1}\hat{h}(2^p\omega)\ \text{ and }\ \hat{\psi}_j(\omega)=\hat{g}(2^{j-L-1}\omega)\prod_{p=0}^{j-L-2}\hat{h}(2^p\omega). \tag{7.145}$$

A filter bank tree of depth $J-L\geq 0$, decomposes a_L over the family of vectors

$$\left[\left\{\phi_J[n-2^{J-L}l]\right\}_{l\in\mathbb{Z}},\left\{\psi_j[n-2^{j-L}l]\right\}_{L<j\leq J,l\in\mathbb{Z}}\right]. \tag{7.146}$$

For conjugate mirror filters, one can verify that this family is an orthonormal basis of $\mathbf{l}^2(\mathbb{Z})$. These discrete vectors are close to a uniform sampling of the continuous time scaling functions $\phi_j(t)=2^{-j/2}\phi(2^{-j}t)$ and wavelets $\psi_j(t)=2^{-j/2}\phi(2^{-j}t)$. When the number $L-j$ of successive convolutions increases, one can verify that $\phi_j[n]$ and $\psi_j[n]$ converge respectively to $N^{1/2}\phi_j(N^{-1}n)$ and $N^{-1/2}\psi_j(N^{-1}n)$. The factor $N^{-1/2}$ normalizes the $\mathbf{l}^2(\mathbb{Z})$ norm of these sampled functions. If $L-j=4$ then $\phi_j[n]$ and $\psi_j[n]$ are already very close to these limit values. The impulse responses $\phi_j[n]$ and $\psi_j[n]$ of the filter bank are thus much closer to continuous time scaling functions and wavelets than they are to the original conjugate mirror filters h and g. This explains why wavelets provide appropriate models for understanding the applications of these filter banks. Chapter 8 relates more general filter banks to wavelet packet bases.

If the decomposition and reconstruction filters of the filter bank are different, the resulting basis (7.146) is non-orthogonal. The stability of this discrete wavelet basis does not degrade when the depth $J-L$ of the filter bank increases. The next section shows that the corresponding continuous time wavelet $\psi(t)$ generates a Riesz basis of $\mathbf{L}^2(\mathbb{R})$.

7.4 BIORTHOGONAL WAVELET BASES [2]

The stability and completeness properties of biorthogonal wavelet bases are described for perfect reconstruction filters h and $\tilde{h}$ having a finite impulse response. The design of linear phase wavelets with compact support is explained in Section 7.4.2.

7.4.1 Construction of Biorthogonal Wavelet Bases

An infinite cascade of perfect reconstruction filters (h,g) and $(\tilde{h},\tilde{g})$ yields two scaling functions and wavelets whose Fourier transforms satisfy

$$\hat{\phi}(2\omega) = \frac{1}{\sqrt{2}}\hat{h}(\omega)\,\hat{\phi}(\omega)\ ,\ \widehat{\tilde{\phi}}(2\omega)=\frac{1}{\sqrt{2}}\widehat{\tilde{h}}(\omega)\,\widehat{\tilde{\phi}}(\omega)\ , \tag{7.147}$$

$$\hat{\psi}(2\omega) = \frac{1}{\sqrt{2}}\hat{g}(\omega)\,\hat{\phi}(\omega)\ ,\ \widehat{\tilde{\psi}}(2\omega)=\frac{1}{\sqrt{2}}\widehat{\tilde{g}}(\omega)\,\widehat{\tilde{\phi}}(\omega)\ . \tag{7.148}$$

In the time domain, these relations become

$$\phi(t) = \sqrt{2}\sum_{n=-\infty}^{+\infty}h[n]\,\phi(2t-n)\ ,\ \tilde{\phi}(t)=\sqrt{2}\sum_{n=-\infty}^{+\infty}\tilde{h}[n]\,\tilde{\phi}(2t-n) \tag{7.149}$$

$$\psi(t) = \sqrt{2}\sum_{n=-\infty}^{+\infty}g[n]\,\phi(2t-n)\ ,\ \tilde{\psi}(t)=\sqrt{2}\sum_{n=-\infty}^{+\infty}\tilde{g}[n]\,\tilde{\phi}(2t-n)\ . \tag{7.150}$$

The perfect reconstruction conditions are given by Theorem 7.9. If we normalize the gain and shift to $a = 1$ and $l = 0$, the filters must satisfy

$$\hat{h}^*(\omega)\,\widehat{\bar{h}}(\omega) + \hat{h}^*(\omega+\pi)\,\widehat{\bar{h}}(\omega+\pi) = 2, \tag{7.151}$$

and

$$\hat{g}(\omega) = \mathrm{e}^{-\mathrm{i}\omega}\,\widehat{\bar{h}}^*(\omega+\pi)\ , \quad \widehat{\bar{g}}(\omega) = \mathrm{e}^{-\mathrm{i}\omega}\,\hat{h}^*(\omega+\pi). \tag{7.152}$$

Wavelets should have a zero average, which means that $\hat{\psi}(0) = \widehat{\bar{\psi}}(0) = 0$. This is obtained by setting $\hat{g}(0) = \widehat{\bar{g}}(0) = 0$ and hence $\hat{h}(\pi) = \widehat{\bar{h}}(\pi) = 0$. The perfect reconstruction condition (7.151) implies that $\hat{h}^*(0)\,\widehat{\bar{h}}(0) = 2$. Since both filters are defined up to multiplicative constants respectively equal to λ and λ^{-1}, we adjust λ so that $\hat{h}(0) = \widehat{\bar{h}}(0) = \sqrt{2}$.

In the following, we also suppose that h and $\bar{h}$ are finite impulse response filters. One can then prove [21] that

$$\hat{\phi}(\omega) = \prod_{p=1}^{+\infty} \frac{\hat{h}(2^{-p}\omega)}{\sqrt{2}} \quad \text{and} \quad \widehat{\bar{\phi}}(\omega) = \prod_{p=1}^{+\infty} \frac{\widehat{\bar{h}}(2^{-p}\omega)}{\sqrt{2}} \tag{7.153}$$

are the Fourier transforms of distributions of compact support. However, these distributions may exhibit wild behavior and have infinite energy. Some further conditions must be imposed to guarantee that ϕ and $\bar{\phi}$ are the Fourier transforms of finite energy functions. The following theorem gives sufficient conditions on the perfect reconstruction filters for synthesizing biorthogonal wavelet bases of $\mathbf{L}^2(\mathbb{R})$.

Theorem 7.11 (COHEN, DAUBECHIES, FEAUVEAU) *Suppose that there exist strictly positive trigonometric polynomials $P(\mathrm{e}^{\mathrm{i}\omega})$ and $\bar{P}(\mathrm{e}^{\mathrm{i}\omega})$ such that*

$$\left|\hat{h}\Big(\frac{\omega}{2}\Big)\right|^2 P(\mathrm{e}^{\mathrm{i}\omega/2}) + \left|\hat{h}\Big(\frac{\omega}{2}+\pi\Big)\right|^2 P(\mathrm{e}^{\mathrm{i}(\omega/2+\pi)}) = 2P(\mathrm{e}^{\mathrm{i}\omega}), \tag{7.154}$$

$$\left|\widehat{\bar{h}}\Big(\frac{\omega}{2}\Big)\right|^2 \bar{P}(\mathrm{e}^{\mathrm{i}\omega/2}) + \left|\widehat{\bar{h}}\Big(\frac{\omega}{2}+\pi\Big)\right|^2 \bar{P}(\mathrm{e}^{\mathrm{i}(\omega/2+\pi)}) = 2\bar{P}(\mathrm{e}^{\mathrm{i}\omega}) \tag{7.155}$$

and that P and $\bar{P}$ are unique (up to normalization). Suppose that

$$\inf_{\omega\in[\ \pi/2,\pi/2]} |\hat{h}(\omega)| > 0\ , \quad \inf_{\omega\in[-\pi/2,\pi/2]} |\widehat{\bar{h}}(\omega)| > 0. \tag{7.156}$$

- *Then the functions $\hat{\phi}$ and $\widehat{\bar{\phi}}$ defined in (7.153) belong to $\mathbf{L}^2(\mathbb{R})$, and ϕ, $\bar{\phi}$ satisfy biorthogonal relations*

$$\langle \phi(t), \bar{\phi}(t-n)\rangle = \delta[n]. \tag{7.157}$$

- *The two wavelet families $\{\psi_{j,n}\}_{(j,n)\in\mathbb{Z}^2}$ and $\{\bar{\psi}_{j,n}\}_{(j,n)\in\mathbb{Z}^2}$ are biorthogonal Riesz bases of $\mathbf{L}^2(\mathbb{R})$.*

The proof of this theorem is in [131] and [21]. The hypothesis (7.156) is also imposed by Theorem 7.2, which constructs orthogonal bases of scaling functions. The conditions (7.154) and (7.155) do not appear in the construction of wavelet orthogonal bases because they are always satisfied with $P(\mathrm{e}^{\mathrm{i}\omega}) = \bar{P}(\mathrm{e}^{\mathrm{i}\omega}) = 1$ and one can prove that constants are the only invariant trigonometric polynomials [247].

Biorthogonality means that for any $(j, j', n, n') \in \mathbb{Z}^4$,

$$\langle \psi_{j,n}, \bar{\psi}_{j',n'}\rangle = \delta[n-n']\,\delta[j-j']. \tag{7.158}$$

Any $f \in \mathbf{L}^2(\mathbb{R})$ has two possible decompositions in these bases:

$$f = \sum_{n,j=-\infty}^{+\infty} \langle f, \psi_{j,n}\rangle\, \bar{\psi}_{j,n} = \sum_{n,j=-\infty}^{+\infty} \langle f, \bar{\psi}_{j,n}\rangle\, \psi_{j,n}\ . \tag{7.159}$$

The Riesz stability implies that there exist $A > 0$ and $B > 0$ such that

$$A\,\|f\|^2 \ \leq \sum_{n,j=-\infty}^{+\infty} |\langle f, \bar{\psi}_{j,n}\rangle|^2 \leq B\,\|f\|^2. \tag{7.160}$$

$$\frac{1}{B}\,\|f\|^2 \ \leq \sum_{n,j=-\infty}^{+\infty} |\langle f, \bar{\psi}_{j,n}\rangle|^2 \leq \frac{1}{A}\,\|f\|^2. \tag{7.161}$$

Multiresolutions Biorthogonal wavelet bases are related to multiresolution approximations. The family $\{\phi(t-n)\}_{n\in\mathbb{Z}}$ is a Riesz basis of the space $\mathbf{V}_0$ it generates, whereas $\{\bar{\phi}(t-n)\}_{n\in\mathbb{Z}}$ is a Riesz basis of another space $\bar{\mathbf{V}}_0$. Let $\mathbf{V}_j$ and $\bar{\mathbf{V}}_j$ be the spaces defined by

$$f(t) \in \mathbf{V}_j \ \Leftrightarrow\ f(2^j t) \in \mathbf{V}_0,$$
$$f(t) \in \bar{\mathbf{V}}_j \ \Leftrightarrow\ f(2^j t) \in \bar{\mathbf{V}}_0.$$

One can verify that $\{\mathbf{V}_j\}_{j\in\mathbb{Z}}$ and $\{\bar{\mathbf{V}}_j\}_{j\in\mathbb{Z}}$ are two multiresolution approximations of $\mathbf{L}^2(\mathbb{R})$. For any $j \in \mathbb{Z}$, $\{\psi_{j,n}\}_{n\in\mathbb{Z}}$ and $\{\phi_{j,n}\}_{n\in\mathbb{Z}}$ are Riesz bases of $\mathbf{V}_j$ and $\bar{\mathbf{V}}_j$. The dilated wavelets $\{\psi_{j,n}\}_{n\in\mathbb{Z}}$ and $\{\bar{\psi}_{j,n}\}_{n\in\mathbb{Z}}$ are bases of two detail spaces $\mathbf{W}_j$ and $\bar{\mathbf{W}}_j$ such that

$$\mathbf{V}_j \oplus \mathbf{W}_j = \mathbf{V}_{j-1} \ \text{ and } \ \bar{\mathbf{V}}_j \oplus \bar{\mathbf{W}}_j = \bar{\mathbf{V}}_{j-1}\ .$$

The biorthogonality of the decomposition and reconstruction wavelets implies that $\mathbf{W}_j$ is not orthogonal to $\mathbf{V}_j$ but is to $\bar{\mathbf{V}}_j$ whereas $\bar{\mathbf{W}}_j$ is not orthogonal to $\bar{\mathbf{V}}_j$ but is to $\mathbf{V}_j$.

Fast Biorthogonal Wavelet Transform The perfect reconstruction filter bank studied in Section 7.3.2 implements a fast biorthogonal wavelet transform. For any discrete signal input $b[n]$ sampled at intervals $N^{-1} = 2^L$, there exists $f \in \mathbf{V}_L$ such that $a_L[n] = \langle f, \phi_{L,n} \rangle = N^{-1/2} b[n]$. The wavelet coefficients are computed by successive convolutions with $\bar{h}$ and $\bar{g}$. Let $a_j[n] = \langle f, \phi_{j,n} \rangle$ and $d_j[n] = \langle f, \psi_{j,n} \rangle$. As in Theorem 7.7, one can prove that

$$a_{j+1}[n] = a_j \star \bar{h}[2n] \quad , \quad d_{j+1}[n] = a_j \star \bar{g}[2n] \quad . \tag{7.162}$$

The reconstruction is performed with the dual filters $\tilde{h}$ and $\tilde{g}$:

$$a_j[n] = \tilde{a}_{j+1} \star \tilde{h}[n] + \tilde{d}_{j+1} \star \tilde{g}[n]. \tag{7.163}$$

If a_L includes N non-zero samples, the biorthogonal wavelet representation $[\{d_j\}_{L<j\leq J}, a_J]$ is calculated with $O(N)$ operations, by iterating (7.162) for $L \leq j < J$. The reconstruction of a_L by applying (7.163) for $J > j \geq L$ requires the same number of operations.

7.4.2 Biorthogonal Wavelet Design [2]

The support size, the number of vanishing moments, the regularity and the symmetry of biorthogonal wavelets is controlled with an appropriate design of h and $\tilde{h}$.

Support If the perfect reconstruction filters h and $\tilde{h}$ have a finite impulse response then the corresponding scaling functions and wavelets also have a compact support. As in Section 7.2.1, one can show that if $h[n]$ and $\tilde{h}[n]$ are non-zero respectively for $N_1 \leq n \leq N_2$ and $\tilde{N}_1 \leq n \leq \tilde{N}_2$, then ϕ and $\tilde{\phi}$ have a support respectively equal to $[N_1, N_2]$ and $[\tilde{N}_1, \tilde{N}_2]$. Since

$$g[n] = (-1)^{1-n} h[1-n] \text{ and } \tilde{g}[n] = (-1)^{1-n} \tilde{h}[1-n],$$

the supports of ψ and $\tilde{\psi}$ defined in (7.150) are respectively

$$\left[\frac{N_1 - \tilde{N}_2 + 1}{2}, \frac{N_2 - \tilde{N}_1 + 1}{2}\right] \text{ and } \left[\frac{\tilde{N}_1 - N_2 + 1}{2}, \frac{\tilde{N}_2 - N_1 + 1}{2}\right]. \tag{7.164}$$

Both wavelets thus have a support of the same size and equal to

$$I = \frac{N_2 - N_1 + \tilde{N}_2 - \tilde{N}_1}{2}. \tag{7.165}$$

Vanishing Moments The number of vanishing moments of ψ and $\tilde{\psi}$ depends on the number of zeros at $\omega = \pi$ of $\hat{h}(\omega)$ and $\widehat{\tilde{h}}(\omega)$. Theorem 7.4 proves that ψ has $\bar{p}$ vanishing moments if the derivatives of its Fourier transform satisfy $\hat{\psi}^{(k)}(0) = 0$ for $k \leq \bar{p}$. Since $\hat{\phi}(0) = 1$, (7.4.1) implies that it is equivalent to impose that $\hat{g}(\omega)$ has a zero of order $\bar{p}$ at $\omega = 0$. Since $\hat{g}(\omega) = e^{-i\omega} \widehat{\tilde{h}}^*(\omega + \pi)$, this means that $\widehat{\tilde{h}}(\omega)$ has a zero of order $\bar{p}$ at $\omega = \pi$. Similarly the number of vanishing moments of $\tilde{\psi}$ is equal to the number $\tilde{p}$ of zeros of $\hat{h}(\omega)$ at π.

Regularity Although the regularity of a function is a priori independent of the number of vanishing moments, the smoothness of biorthogonal wavelets is related to their vanishing moments. The regularity of ϕ and ψ is the same because (7.150) shows that ψ is a finite linear expansion of ϕ translated. Tchamitchian's Proposition 7.3 gives a sufficient condition for estimating this regularity. If $\hat{h}(\omega)$ has a zero of order p at π, we can perform the factorization

$$\hat{h}(\omega) = \left(\frac{1 + e^{-i\omega}}{2}\right)^p \hat{l}(\omega). \tag{7.166}$$

Let $B = \sup_{\omega \in [-\pi,\pi]} |\hat{l}(\omega)|$. Proposition 7.3 proves that ϕ is uniformly Lipschitz α for

$$\alpha < \alpha_0 = p - \log_2 B - 1.$$

Generally, $\log_2 B$ increases more slowly than p. This implies that the regularity of ϕ and ψ increases with p, which is equal to the number of vanishing moments of $\tilde{\psi}$. Similarly, one can show that the regularity of $\tilde{\psi}$ and $\tilde{\phi}$ increases with $\tilde{p}$, which is the number of vanishing moments of ψ. If $\hat{h}$ and $\tilde{h}$ have different numbers of zeros at π, the properties of ψ and $\tilde{\psi}$ can therefore be very different.

Ordering of Wavelets Since ψ and $\tilde{\psi}$ might not have the same regularity and number of vanishing moments, the two reconstruction formulas

$$f = \sum_{n,j=-\infty}^{+\infty} \langle f, \psi_{j,n} \rangle \tilde{\psi}_{j,n}, \tag{7.167}$$

$$f = \sum_{n,j=-\infty}^{+\infty} \langle f, \tilde{\psi}_{j,n} \rangle \psi_{j,n} \tag{7.168}$$

are not equivalent. The decomposition (7.167) is obtained with the filters (h, g) at the decomposition and $(\tilde{h}, \tilde{g})$ at the reconstruction. The inverse formula (7.168) corresponds to $(\tilde{h}, \tilde{g})$ at the decomposition and (h, g) at the reconstruction.

To produce small wavelet coefficients in regular regions we must compute the inner products using the wavelet with the maximum number of vanishing moments. The reconstruction is then performed with the other wavelet, which is generally the smoothest one. If errors are added to the wavelet coefficients, for example with a quantization, a smooth wavelet at the reconstruction introduces a smooth error. The number of vanishing moments of ψ is equal to the number $\bar{p}$ of zeros at π of $\widehat{\tilde{h}}$. Increasing $\bar{p}$ also increases the regularity of $\tilde{\psi}$. It is thus better to use h at the decomposition and $\tilde{h}$ at the reconstruction if $\tilde{h}$ has fewer zeros at π than $\widehat{\tilde{h}}$.

Symmetry It is possible to construct smooth biorthogonal wavelets of compact support which are either symmetric or antisymmetric. This is impossible for orthogonal wavelets, besides the particular case of the Haar basis. Symmetric or